PFC/JA-89-15

# WAVEGUIDE MODE DEFORMATION IN FREE ELECTRON LASERS

J. Fajans* and J.S. Wurtele

February, 1989

Plasma Fusion Center
Massachusetts Institute of Technology
Cambridge, Massachusetts 02139 USA

*Present address: Department of Physics, University of California, Berkeley, California 94720

This work was supported by the National Science Foundation, the Office of Naval Research and the Department of Energy, Office of High Energy Physics.

February 15, 1989

# Waveguide Mode Deformation in Free Electron Lasers

J. Fajans
Department of Physics
University of California, Berkeley
Berkeley, California 94720
J.S. Wurtele
Department of Physics and Plasma Fusion Center
Massachusetts Institute of Technology
Cambridge, Massachusetts 02139

We calculate the free-electron laser (FEL) induced modifications to the vacuum waveguide modes for low frequency FELs. Typically, the mode modifications are large, and exhibit complicated axial behaviors. In addition to the wave component with a near vacuum wavenumber, components at two upshifted wavenumbers must be analysed. Electron beam surface charges and currents are also important. At low gain, effects from all three roots of the FEL dispersion relation must be included. The dominant modification is due to the electron beam space charge wave.

# I. Introduction

The free electron laser (FEL) is an efficient source of tunable coherent radiation. Since the FEL was first envisioned,[1,2] lasing has been achieved from visible to microwave frequencies,[3] and the theoretical understanding of FELs has increased proportionately. Experimental measurements of wave amplitude and phase are in good agreement with theory in both the linear and nonlinear regimes.[4,5] To control the electromagnetic radiation wave, experiments employ waveguides or optical cavities. When cavities are used, the vacuum interaction length is of the order of one Rayleigh range; however, many planned and in progress optical wavelength FELs require interaction lengths of many Rayleigh ranges. To maintain strong coupling between the wave and the electron beam, these experiments must rely on the predicted phenomenon of optical guiding.

Optical guiding,[6-11] is expected to occur when the FEL interaction produces an index of refraction greater than unity. Since the wave phase velocity is then slowed inside the electron beam, the beam will guide the radiation in a manner similar to the guiding of light by an optical fiber. Consequently the wave does not diffract as it would in the absence of the FEL interaction, and interaction lengths of many Rayleigh ranges are predicted. Optical guiding is particularly important for both high efficiency lasers operating at infrared and shorter wavelengths, and for lasers which amplify spontaneous emission at extreme ultraviolet and shorter wavelengths. Numerous experimental efforts are underway to verify the optical guiding effect. Measurements of the wave phase, which is related to FEL induced changes in real part of the index of refraction, have been made using interferometric techniques.[5,12] Experiments have attempted to measure mode profile changes directly.[13-15] Bending effects in FEL oscillators[16] may also be due to optical guiding effects.

When the electromagnetic wavelength is large, the wave must be guided by an external structure; typically a waveguide is employed. Consequently, experiments operating at these wavelengths cannot observe "classical" optical guiding. Even when optical guiding effects are strong, the radiation is never completely confined to the electron beam, and the waveguide remains important. However, the transverse structure of the electromagnetic radiation is modified by the FEL interaction. Physically, this modification is the waveguide analog of optical guiding; the electron beam undergoing the FEL

interaction generates an index of refraction which changes the mode profile. The purpose of this paper is to analyze these changes in the field profile during the FEL interaction.

Motivation for this paper comes from several experiments, including measurements of the mode composition in an overmoded oscillator[13] and direct measurements of the transverse electric field in an FEL amplifier operating with a only one vacuum mode above cutoff.[14] These experiments show that substantial mode profile modifications occur. We will show that the mode profile changes are influenced by both space charge and electromagnetic effects, and that the space charge fields can dominate the profile modifications.

The following simple argument demonstrates that the profile modifications in a waveguide FEL may be large. The relation between the normalized wavenumber shift, $\delta k/k$, due to a dielectric in a waveguide excited by frequency $\omega$ is given by the perturbation formula[17]

$$\frac{\delta k}{k} = \frac{\omega^2}{c^2 k^2} \frac{\int \Delta\epsilon E^2 \, dS}{\int (\epsilon_0 E^2 + \mu_0 H^2) \, dS}.$$

When the electron beam radius is much smaller than the waveguide radius, the expression for $\delta k/k$ becomes

$$\frac{\delta k}{k} \sim \frac{A_{\rm eb}}{A_{\rm wg}} \Delta\epsilon .$$

Consequently $\Delta\epsilon \sim (A_{\rm wg}/A_{\rm eb})\delta k/k$, where $A_{\rm wg}$ and $A_{\rm eb}$ are, respectively, the areas of the waveguide and the electron beam. Free electron lasers operating at low frequencies can have ratios of $\delta k/k \geq 0.03$.[18-20] If the beam area ratio is 25,[18] the dielectric constant would be 1.75. Thus these FELs have a significant perturbed dielectric constant, and we would anticipate strong local perturbations to the waveguide mode in the region of the electron beam. This picture is, of course, far too simplistic to accurately model the perturbed fields. While an appropriate dielectric constant can be constructed,[21] it has complicated tensor properties and is not well described by the isotropic dielectric constant discussed above. (In addition, as discussed in the next paragraph, the electron beam also generates fields which vary with wavenumbers other than the input wavenumber. These "parasitic" emenations are difficult to model with a dielectric).

In one set of experiments[14] designed to study the mode profile changes, the electric field is measured as function of transverse position. Most of the radiation power is carried by an electromagnetic wave whose profile is close to, but not identical to the profile of a standard vacuum waveguide mode. This wave propagates with wavenumber $k_z + \delta k$, where $k_z$ is the axial wavenumber of the appropriate vacuum waveguide mode, and $\delta k$ is the FEL induced wave phase shift. The FEL space-charge induced fields propagate with the wavenumber $k_z + k_w + \delta k$, where $k_w = 2\pi/l_w$, and $l_w$ is wiggler wavelength. There is also a second electromagnetic mode with wavenumber $k_z + 2k_w + \delta k$. Furthermore, the wiggling motion and the bunching in the ponderomotive wave results in psuedo surface charge and surface current generated components of the electric field which vary with the axial wavenumbers $k_z + \delta k$ and $k_z + 2k_w + \delta k$. All these components will interfere with each other, causing the details of the observed mode profile to depend on the axial position.

Our model, presented in Sec. II, assumes that, in the absence of the electron beam, the radiation propagates in a standard vacuum waveguide mode. For simplicity, we give examples for the $TE_{11}$ waveguide mode. Next we postulate an electron beam with a density modulation due to the FEL interaction, characterized by the induced phase shift $\delta k$. The beam is assumed uniform out to the beam radius and independent of azimuthal angle. We then assume that the beam is undulated by the FEL wiggler. Finally, straightforward calculations yield the three dimensional electric and magnetic field profile. To calculate $\delta k$ we employ an extended one dimensional linear theory,[5,4,22] in which the radiation and space-charge wave coupling coefficient are calculated using overlap integrals and a space-charge reduction parameter,[23] to explicitly determine the axial wavenumbers of the beam density modulation. In the high gain regime, the mode with the exponentially growing root of the cubic FEL dispersion relation dominates the interaction, but in the low gain regime all of the FEL cubic roots must be retained.[24] Note that we require an accurate value for the induced phase shift. Since we postulate $\delta k$, our approach is not fully self-consistent, but it has the virtue that the equations for the fields can be easily interpreted. In section III we plot the fields under different conditions. We discuss scaling and self consistancy in Section IV, and conclude in section V.

Our derivation, which is valid in both the Compton and the Raman (collective) regimes, resembles, in some respects, earlier work by Freund and

Ganguly,[22] and Uhm and Davidson.[25] However, the emphasis in these works was the calculation of the FEL gain, and the authors did not explicitly construct the wave profiles. The authors considered either idealized, nonphysical "shell" electron beams, rather than realizable solid electron beams, or considered only Compton FELs. The case of a Raman FEL with a solid electron beam was not examined. Fruchtman studied a sheet-beam FEL.[31] Many workers[26-30] have developed particle simulations to model the FEL in a waveguide. As with many optical guiding calculations, these nonlinear simulations do not treat the full three dimensional nature of the electrostatic mode. The axial space charge electric field is generally used only in the longitudinal particle dynamics, and the radial component of this field is neglected in calculating the local electric field profile and the transverse particle dynamics. Some simulations expand the transverse field in a sum of vacuum waveguide modes. Such expansions do not allow for any surface charge effects, because, by construction, these expansions do not include modes for which $\nabla \cdot \vec{E} \neq 0$. However, as discussed above, there are additional modifications to the field at the RF wavenumber $k_z + \delta k$, due to the pseudo surface charge generated components. Consequently such methods cannot include the full, rich range of profile modification phenomena. More recently, in a paper[21] which complements this work, the linear kinetic theory of the raman FEL in waveguides has been analyzed.

## II. Basic Theory

In this section, we calculate the mode deformation for a wiggling electron beam which is axially modulated and has a uniform transverse density profile. The electron beam, with axial velocity $v_z$ and radius $b$, propagates in a circular waveguide of radius $a$ (Fig. 1). A wiggler field causes the electron beam to helically undulate with period $l_w$, so that the total beam velocity is

$$\mathbf{v} = v_z\hat{z} + v_w(\hat{x}\cos k_w z - \hat{y}\sin k_w z) \tag{1}$$

where $k_w = 2\pi/l_w$ is the wiggler wavenumber, and $v_w$ is the wiggler induced transverse velocity. Here, and in the rest of this paper, three dimensional wiggler effects are ignored. The electron beam is assumed to be axially modulated with amplitude $C$, thus

$$\rho = u(b-r)[Ce^{i(\omega t-(k_z+\delta k+k_w)z)} + \text{c.c.}]\,, \tag{2}$$

where $u$ is the Heaviside function, and $\omega$ is the frequency of the incident radiation. The unperturbed wavenumber, $k_z$, of the incident radiation depends on the particular waveguide mode in which the radiation propagates. The radius $b$ of the electron beam is taken to be constant in Eq. 2, and this approximation will result (Eq. 22) in a surface charge density and a surface current at the beam boundary.

In addition to the density modulation $\rho$ of Eq. 2, linear FEL theory also yields a perturbed velocity, $\vec{v}_1$. The synchronous current component which results from this velocity modulation is, however, substantially smaller than the synchronous current which arrises from the density modulation. In our analysis, therfore, the fields are driven only by those currents which result from density modulation and the wiggling motion.

The FEL interaction induces the wavenumber shift $\delta k$ and also determines the amplitude $C$ of the density perturbation. In general, each of the three roots of the FEL dispersion relation has a different value of $\delta k$, and generates a correspondingly different perturbed density of the form of Eq. 2. Since the Maxwell equations are linear, the total field can be calculated by summation of the fields which are produced from each of the three components of the total density perturbation. The parameters $\delta k$ and $C$ are given by one dimensional theories; appropriate values for these constants and details of the superposition of perturbations with differing $\delta k$ will be discussed in section IIIb.

The modulated electron beam has a rapidly oscillating current density

$$\mathbf{J} = \rho \mathbf{v} = J_z \hat{z} + \mathbf{J}_\perp, \tag{3}$$

where, using Eqs. 1 and 2 and transforming to cylindrical coordinates $(\hat{r}, \hat{\phi}, \hat{z})$

$$\begin{aligned} J_z &= v_z u(b-r)[Ce^{i(\theta - k_w z)} + \text{c.c.}] \\ \mathbf{J}_\perp &= \frac{1}{2} v_w u(b-r)\left[\hat{r}(j_0 e^{i\phi} + j_2 e^{-i\phi}) + i\hat{\phi}(j_0 e^{i\phi} - j_2 e^{-i\phi}) + \text{c.c.}\right]. \end{aligned} \tag{4}$$

In Eq. 4,

$$j_0 = Ce^{i\theta}, \qquad j_2 = Ce^{i(\theta - 2k_w z)}, \tag{5}$$

and $\theta$ is the phase angle $\theta = \omega t - (k_z + \delta k)z$.

Combining Ampere's law and Faraday's law in the standard way forms the driven Helmholtz equation

$$\nabla^2 \mathbf{E} + k_v^2 \mathbf{E} = ik_v Z_0 \mathbf{J} + \nabla \rho / \epsilon_0. \tag{6}$$

Using the continuity equation, Eq. 6 can be reexpressed as

$$(\nabla^2 + k_v^2)\mathbf{E} = ik_v Z_0 \left[\mathbf{J} + \frac{1}{k_v^2}\nabla(\nabla \cdot \mathbf{J})\right], \tag{7}$$

where the RHS has the convenient property that it depends on J only. Here $k_v = \omega/c$, where $c$ is the speed of light, and $Z_0 = \sqrt{\mu_0/\epsilon_0}$.

The FEL induced waveguide mode deformation is found by substituting the driving currents Eq. 4 into the modified Helmholtz Eq. 7. An examination of Eq. 4 shows that the driving currents naturally divide into three groups: an axial ($\hat{z}$-directed) current with phase $\theta - k_w z$, and two transverse currents, one with phase $\theta$ and the other with phase $\theta - 2k_w z$. These currents are not cross coupled by the Helmholtz equation; thus the mode profile from each current can be calculated separately and the results superimposed to yield the full mode corresponding to an electron beam with the velocity given by Eq. 1 and the density given by Eq. 2.

## A. Axial current modes

The fields due to the axially directed current $J_z$ are readily identified as the space-charge wave fields. The electric field is assumed to be of the form $\mathbf{E}_1 \exp(i(\theta - k_w z)) + \text{c.c.}$, and from here on the complex conjugate term will be dropped. Inserting the expression for $\mathbf{E}_1$ into the Helmholtz equation (Eq. 7) and factoring out the time dependance gives

$$(\nabla^2 + k_v^2)\mathbf{E}_1 e^{-ik_1 z} = ik_v Z_0 v_z C u(b - r)\left[1 - \frac{k_1^2}{k_v^2}\right] e^{-ik_1 z}, \tag{8}$$

where the axial wavenumber is $k_1 = k_z + \delta k + k_w$. For $r < b$ the inhomogeneous solution of this equation is

$$\mathbf{E}_{1,\mathrm{i}} = \frac{iZ_0 v_z C}{k_v} e^{-ik_1 z}\hat{z} \qquad r < b \tag{9}$$

and the corresponding inhomogeneous magnetic field is equal to zero.

In order to satisfy the boundary conditions at $r = b$, an appropriate solution of the homogeneous equation

$$(\nabla^2 + k_v^2)\mathbf{E}_{1,\mathrm{h}} e^{-ik_1 z} = 0 \tag{10}$$

| Fields from the Axial Current | | |
|---|---|---|
| | In | Out |
| $\mathbf{E}_r$ | $BJ_1(k_{1r}r)e^{-ik_1z}$ | $A\left[J_1(k_{1r}r)+\alpha_1 Y_1(k_{1r}r)\right]e^{-ik_1z}$ |
| $\mathbf{E}_\phi$ | 0 | 0 |
| $\mathbf{E}_z$ | $-iB(k_{1r}/k_1)J_0(k_{1r}r)e^{-ik_1z}$ | $-iA(k_{1r}/k_1)\left[J_0(k_{1r}r)+\alpha_1 Y_0(k_{1r}r)\right]e^{-ik_1z}$ |
| $\mathbf{H}_r$ | 0 | 0 |
| $\mathbf{H}_\phi$ | $(B/Z_1)J_1(k_{1r}r)$ | $(A/Z_1)\left[J_1(k_{1r}r)+\alpha_1 Y_1(k_{1r}r)\right]e^{-ik_1z}$ |
| $\mathbf{H}_z$ | 0 | 0 |
| $Z_1 = k_1 Z_0/k_v$ . | | |

Table 1: Fields driven by the axially directed beam current.

must be found by matching the solutions of Eq. 10 across the beam boundary. The complete solution will be

$$\mathbf{E}_1 = \begin{cases} \mathbf{E}^{<}_{1,\mathrm{h}} + \mathbf{E}_{1,\mathrm{i}} & r < b \\ \mathbf{E}^{>}_{1,\mathrm{h}} & b < r < a \end{cases}, \tag{11}$$

and

$$\mathbf{H}_1 = \begin{cases} \mathbf{H}^{<}_{1,\mathrm{h}} & r < b \\ \mathbf{H}^{>}_{1,\mathrm{h}} & b < r < a \end{cases}. \tag{12}$$

The general form of the homogeneous fields are given by the well known Bessel functions shown in Table 1, where we have defined the radial wavenumber $k_{1r} = \sqrt{k_v^2 - k_1^2}$.

For perfectly conducting waveguide walls, $E_z(r = a) = 0$. Thus the coefficient $\alpha_1$ in Table 1 is

$$\alpha_1 = -\frac{J_0(k_{1r}a)}{Y_0(k_{1r}a)}. \tag{13}$$

Because the gradient of $J_z$ is continuous across the beam boundary at $r = b$, there is no charge layer on the beam surface; consequently the electric field must be continuous across the beam boundary. This leads to two conditions, one on $\mathbf{E}_z$

$$A\left[J_0(k_{1r}b)+\alpha_1 Y_0(k_{1r}b)\right] - BJ_0(k_{1r}b) = -\frac{v_z \mathcal{C} Z_1}{k_{1r}}, \tag{14}$$

and one on $\mathbf{E}_r$

$$A\left[J_1(k_{1r}b) + \alpha_1 Y_1(k_{1r}b)\right] - BJ_1(k_{1r}b) = 0. \tag{15}$$

These two equations are readily solved for $A$ and $B$.

## B. Transverse modes

The solution for the fields produced by the transverse currents is somewhat more complicated than the solution for the axial current. The transverse current is comprised of two components, one with wavenumber $k_z + \delta k$ and the other with wavenumber $k_z + \delta k + 2k_w$, corresponding to the $j_0$ and $j_2$ terms in Eq. 5. Since the method used for the $j_2$ current is nearly identical to the method used for the $j_0$ current, we will only discuss the latter in detail. Assuming the form $\mathbf{E}_0 \exp(i(\omega t - k_0 z))$ for the electric field, inserting this form into the Helmholtz equation (Eq. 7), and factoring out the time dependance results in the relation

$$(\nabla^2 + k_v^2)\mathbf{E}_0 e^{-ik_0 z} = \frac{i}{2} k_v Z_0 v_w C u(b-r)\left(\hat{r}e^{i\phi} + i\hat{\phi}e^{i\phi}\right) e^{-ik_0 z}, \tag{16}$$

where the new axial wavenumber is $k_0 = k_z + \delta k$. The inhomogeneous solution of this equation is

$$\mathbf{E}_{0,\mathrm{i}} = \frac{i}{2}\frac{k_v Z_0 v_w C}{k_{0r}^2} e^{i\phi}\left(\hat{r} + i\hat{\phi}\right) u(b-r) e^{-ik_0 z}. \tag{17}$$

Here the radial wavenumber is $k_{0r} = \sqrt{k_v^2 - k_0^2}$. The corresponding inhomogeneous magnetic field is

$$\mathbf{H}_{0,\mathrm{i}} = \frac{v_w C k_0}{2k_{0r}^2} e^{i\phi}\left(\hat{r} + i\hat{\phi}\right) u(b-r) e^{-ik_0 z}. \tag{18}$$

Once again the boundary conditions at $r = a$ and $r = b$ requires the addition of a solution to the homogeneous equation,

$$(\nabla^2 + k_v^2)\mathbf{E}_{0,\mathrm{h}} e^{-ik_0 z} = 0, \tag{19}$$

The solutions to this equation can be divided into TE-like and TM-like modes, as shown in Tables 2 and 3.

| TE like Fields from the Transverse Current | | |
|---|---|---|
| | In | Out |
| $\mathbf{E}_r$ | $(D/k_{0r}r)J_1(k_{0r}r)e^{i(\phi-k_{0z}z)}$ | $(C/k_{0r}r)\left[J_1(k_{0r}r)+\alpha_{H0}Y_1(k_{0r}r)\right]e^{i(\phi-k_{0z}z)}$ |
| $\mathbf{E}_\phi$ | $iDJ_1'(k_{0r}r)e^{i(\phi-k_{0z}z)}$ | $iC\left[J_1'(k_{0r}r)+\alpha_{H0}Y_1'(k_{0r}r)\right]e^{i(\phi-k_{0z}z)}$ |
| $\mathbf{E}_z$ | 0 | 0 |
| $\mathbf{H}_r$ | $-\mathbf{E}_\phi/Z_{H0}$ | $-\mathbf{E}_\phi/Z_{H0}$ |
| $\mathbf{H}_\phi$ | $\mathbf{E}_r/Z_{H0}$ | $\mathbf{E}_r/Z_{H0}$ |
| $\mathbf{H}_z$ | $D(k_{0r}/Z_{H0}k_0)J_1(k_{0r}r)e^{i(\phi-k_{0z}z)}$ | $C(k_{0r}/Z_{H0}k_0)\left[J_1(k_{0r}r)+\alpha_{H0}Y_1(k_{0r}r)\right]e^{i(\phi-k_{0z}z)}$ |
| $Z_{H0}=k_vZ_0/k_0$ | | |

Table 2: TE fields driven by the transverse beam currents.

| TM like Fields from the Transverse Current | | |
|---|---|---|
| | In | Out |
| $\mathbf{E}_r$ | $FJ_1'(k_{0r}r)e^{i(\phi-k_{0z}z)}$ | $E\left[J_1'(k_{0r}r)+\alpha_{E0}Y_1'(k_{0r}r)\right]e^{i(\phi-k_{0z}z)}$ |
| $\mathbf{E}_\phi$ | $i(F/k_{0r}r)J_1(k_{0r}r)e^{i(\phi-k_0z)}$ | $i(E/k_{0r}r)\left[J_1(k_{0r}r)+\alpha_{E0}Y_1(k_{0r}r)\right]e^{i(\phi-k_0z)}$ |
| $\mathbf{E}_z$ | $iF(k_{0r}/k_0)J_1(k_{0r}r)e^{i(\phi-k_{0z}z)}$ | $iE(k_{0r}/k_0)\left[J_1(k_{0r}r)+\alpha_{E0}Y_1(k_{0r}r)\right]e^{i(\phi-k_{0z}z)}$ |
| $\mathbf{H}_r$ | $-\mathbf{E}_\phi/Z_{E0}$ | $-\mathbf{E}_\phi/Z_{E0}$ |
| $\mathbf{H}_\phi$ | $\mathbf{E}_r/Z_{E0}$ | $\mathbf{E}_r/Z_{E0}$ |
| $\mathbf{H}_z$ | 0 | 0 |
| $Z_{E0}=k_0Z_0/k_v$ | | |

Table 3: TM fields driven by the transverse beam currents.

Equation 19 must be solved inside and outside the electron beam, and then matched across the beam boundary. The complete solution will then be

$$\mathbf{E}_0 = \begin{cases} \mathbf{E}^{<}_{0,\mathrm{h}} + \mathbf{E}_{0,\mathrm{i}} & r < b \\ \mathbf{E}^{>}_{0,\mathrm{h}} & b < r < a \end{cases}, \tag{20}$$

and

$$\mathbf{H}_0 = \begin{cases} \mathbf{H}^{<}_{0,\mathrm{h}} + \mathbf{H}_{0,\mathrm{i}} & r < b \\ \mathbf{H}^{>}_{0,\mathrm{h}} & b < r < a \end{cases}. \tag{21}$$

The boundary matching conditions are complicated by the presence of a surface charge and a surface current layer at the beam edge. The surface charge and current are an artifact of the previous simplification that the beam boundary is fixed at $r = b$. Although this assumption is made in almost all FEL theory, the beam, of course, is not fixed, but instead undulates with the wiggler periodicity and propagates axially. This undulation can be approximated as a surface charge and surface current, and is readily explained by Fig. 2. As show in the top of the figure, the true beam undulates and is density modulated. (For pictorial simplicity, we have chosen the density modulation to have half the period of the undulation, which occurs when $k_z = k_w$). The beam can be split into two superimposed components. The first, shown in the middle of Fig. 2, is a fixed boundary, density modulated beam, and is the only component commonly analyzed. The second component, at the bottom of the figure, consists of all the real and virtual charges required to account for the beam edge oscillation. To retain analytic tractibility we compress this second component into a surface layer of negligible thickness at the fixed beam boundary ($r = b$), resulting in a surface charge and surface current. Note that these charges and currents are composed of components at both $k_z$ and $k_z + 2k_w$.

The continuity equation at the beam boundary $r = b$ must be satisfied. However, this imposes only a non-restrictive condition on the beam surface charge and current; in fact, the continuity equation can be satisfied with a surface current only or a surface charge only. As explained above, the correct surface charge and current are found be compressing the beam and determining the charge and current of the compressed layer. With the undulating velocity defined in Eq. 1, the fluctuation of radius of the beam envelope is

$$\tilde{r}_\perp = \frac{v_w}{k_w v_z} \sin(\phi + k_w z). \tag{22}$$

and, assuming that $\tilde{r}_\perp << b$, the corresponding surface charge density is

$$\begin{aligned} \sigma &= \tilde{r}_\perp \rho \\ &= -i\frac{v_w}{2k_w v_z}\left(j_0 e^{i\phi} - j_2 e^{-i\phi}\right), \end{aligned} \tag{23}$$

where $j_0$ and $j_2$ are defined in Eq. 5. The axial surface current is found to be

$$\begin{aligned} \mathcal{I} &= \tilde{r}_\perp J_z = \sigma v_z \\ &= -i\frac{v_w}{2k_w}\left(j_0 e^{i\phi} - j_2 e^{-i\phi}\right)\hat{z}. \end{aligned} \tag{24}$$

The surface current has an azimuthal as well as an axial component, but the azimuthal component is smaller by a factor $v_w/v_z$, and therefore is neglected in this analysis.

Using the surface charge in Eq. 23 and current in Eq. 24 to determine the jump boundary condition, the matching conditions at $r = b$ are, for the $j_0$ component,

$$\mathbf{E}^{>}_{0,\mathrm{h}} = \mathbf{E}^{<}_{0,\mathrm{h}} + \mathbf{E}_{0,\mathrm{i}} - i\frac{v_w \mathcal{C}}{2k_w v_z \epsilon_0} e^{i\phi}\hat{r}, \tag{25}$$

and

$$\mathbf{H}^{>}_{0,\mathrm{h}} = \mathbf{H}^{<}_{0,\mathrm{h}} + \mathbf{H}_{0,\mathrm{i}} - i\frac{v_w \mathcal{C}}{2k_w} e^{i\phi}\hat{\phi}. \tag{26}$$

These boundary conditions lead to

$$\begin{array}{lrcl} \mathbf{H}_z: & C\left[J_1(k_{0r}b) + \alpha_{\mathrm{H0}} Y_1(k_{0r}b)\right] - D J_1(k_{0r}b) &=& 0 \\ \mathbf{H}_r: & C\left[J_1'(k_{0r}b) + \alpha_{\mathrm{H0}} Y_1'(k_{0r}b)\right] - D J_1'(k_{0r}b) &=& iv_w \mathcal{C} Z_{\mathrm{H0}} k_0/(2k_{0r}^2) \\ \mathbf{E}_z: & E\left[J_1(k_{0r}b) + \alpha_{\mathrm{E0}} Y_1(k_{0r}b)\right] - F J_1(k_{0r}b) &=& 0 \\ \mathbf{H}_\phi: & E\left[J_1'(k_{0r}b) + \alpha_{\mathrm{E0}} Y_1'(k_{0r}b)\right] - F J_1'(k_{0r}b) &=& iv_w \mathcal{C} Z_{\mathrm{E0}} k_0/(2k_{0r}^2) \\ & & & -iv_w \mathcal{C} Z_{\mathrm{E0}}/2k_w \end{array} \tag{27}$$

The additional boundary conditions on $\mathbf{E}_r$ and $\mathbf{E}_\phi$ are redundant. The boundary at the waveguide wall ($r = a$) requires that

$$\alpha_{\mathrm{H0}} = -\frac{J_1'(k_{0r}a)}{Y_1'(k_{0r}a)}, \qquad \alpha_{\mathrm{E0}} = -\frac{J_1(k_{0r}a)}{Y_1(k_{0r}a)} \tag{28}$$

The system of linear equations Eq. 27 is readily solved for $C$,$D$,$E$, and $F$, and the pairs $CD$ and $EF$ do not cross couple. Note that nowhere in this

derivation is the vacuum waveguide mode explicitly specified. The vacuum waveguide mode is indirectly chosen through the value of $k_z$; a value of $k_z$ close to the value for a given vacuum mode will cause the appropriate Bessel functions in Eq. 27 to be near zero, resulting in a large corresponding multiplying coefficient.

The fields from the transverse current $j_2$ can be found by analogy with the solution for $j_0$. We define a new axial wavenumber $k_2 = k_z + \delta k + 2k_w$, a new radial wavenumber $k_{2r} = \sqrt{k_v^2 - k_2^2}$, analogous $Z_{H2}$ and $Z_{E2}$, and use the ansatz $\mathbf{E} = \mathbf{E}_2 \exp(i(\omega t - k_2 z))$. An examination of Eq. 4 shows that the inhomogeneous factors which would multiply $\exp(-ik_2 z)$ in equations analogous to the inhomogeneous Eqs. 16-18 combine in the form $(\hat{r} - i\hat{\phi})\exp(-i\phi)$. Furthermore, the surface charge and surface current, and thus the jump in the field at the beam boundary (see Eq. 25), also vary as $(\hat{r} - i\hat{\phi})\exp(-i\phi)$. The TE and TM modes of Tables 2 and 3 are replaced by by corresponding modes which propagate with $\exp(-ik_2 z)$ and have an $\exp(-i\phi)$ azimuthal variation; also, $\alpha_{H2}$ and $\alpha_{E2}$ are analagously defined. The new boundary conditions can then be derived, are almost identical in form to Eq. 27. The only changes in the boundary condition are that the RHS of the $H_r$ boundary equation and the second term (which arises from the surface current) on the RHS of the $H_\phi$ boundary equation are both multiplied by $-1$.

## III. Mode deformation

The method of solution developed above requires that the values of $\delta k$ and $C$ are known from a quasi-one dimensional theory, in which three dimensional effects are included by the calculation of appropriate overlap parameters. Since such theories are in excellent agreement with experimental results,[5] the assumption that the complete inclusion of three dimensional effects will produce only small changes in the parameters $\delta k$ and $C$ appears warranted.

Free electron lasers operate in both the linear and nonlinear regimes, and, especially in the low gain regime, several FEL modes (several $\delta k$, $C$) may be simultaneously important. An accurate description of the interaction requires the initial value problem be solved through a Laplace transform technique.[24]

## A. Field profile with a single FEL mode

Linear, one dimensional FEL theory is normally based on solving the cubic equation

$$\delta k\,(\delta k - \Theta + \Theta_p)\,(\delta k - \Theta - \Theta_p) + Q = 0, \tag{29}$$

where $\Theta$ is the FEL energy detuning, $\Theta_p$ is the normalized plasma frequency, and $Q$ is the coupling constant. While this equation is inherently one dimensional, three dimensional effects can be included by multiplying the basic coupling constant by an overlap integral, and by reducing the plasma frequency because of the finite size of the electron beam and the presence of the perfectly conducting waveguide walls. This cubic has three solutions, leading to three distinct FEL modes. The fraction of the input power that couples into each FEL mode is a function of the detuning, and can be found by solving the initial value problem. In this section we assume that only a single FEL mode contributes significantly to transverse profile modification, and therefore only one $\delta k$ need be considered. The case of three FEL modes will be discussed in the next section.

A consequence of the assumption that the FEL has infinite longitudinal extent and that $\delta k$ is independent of $z$ is that the electromagnetic radiation supported by the postulated beam density perturbation will have the same transverse profile at all values of $z$ having the same phase in the wiggler (i.e., $k_w z$ differing by a multiple of $2\pi$). This transverse profile is, of course, multiplied by an overall constant which determines its local, instantaneous phase and magnitude. This constant is proportional to the amplitude of the beam perturbation $C$; thus $C$ merely fixes the initial magnitude and phase of the electromagnetic wave. It does not effect the transverse profile. This freedom in the choice of $C$ allows us to specify the amplitude and phase of the electromagnetic wave at any arbitrary position. It is most convenient to choose the magnitude of $C$ so that, at $z = 0$, the electromagnetic power carried by the wave is unity, and to choose the phase of $C$ so that the EM wave phase at $t, z = 0$ is zero. We find that the substitution $C = \delta k \tilde{C}$, where $\tilde{C}$ is, to first order, independent of $\delta k$, makes the electromagnetic power independent of $\delta k$. This substitution can be motivated by solving the complete FEL problem, and noting that the beam density perturbation is proportional to $\delta k$. (The beam density is proportional to $\delta k$ since, from

the eikonal form of the wave equation used in one dimensional FEL theory,[4] $i\delta kE \propto \langle \exp i(\omega t - (k_z + k_w)z) \rangle \propto \tilde{\rho})$.

Experimentally only the total electromagnetic field can be observed. However, since each of the three driving currents of the previous section has a different wavenumber ($k_z+\delta k$ ($k_0$ current), $k_z+\delta k+k_w$ ($k_1$ current) $k_z+\delta k+2k_w$ ($k_2$ current)), it is useful to separately display the fields driven by each current. The different wavenumbers cause the respective fields to superimpose with varying degrees of constructive and destructive interference. When the common periodicity $k_z + \delta k = k_0$ is factored out, the field generated by the $k_0$ current is invariant, the field of the $k_1$ current has the period $l_w$ (the wiggler period), and the field of the $k_2$ current has the period $l_w/2$. As we will show in Fig. 6, within one wiggler period the total field profile has eight characteristic shapes.

In Figs. 3-5 we plot the transverse profiles for each of the field components. The FEL parameters are typical of the experiment described in Ref. 14. The waveguide radius is $b = 1.27$cm, the beam radius is $a = 0.254$cm, and the frequency, $f = 11$GHz, is relatively close to the waveguide cutoff frequency of 6.9GHz. The wiggler period is $l_w = 3.3$cm, and the normalized beam velocities are $\beta_z = 0.624$ and $\beta_\perp = 0.1$. To highlight the profile modifications, we choose a large wavenumber shift of $|\delta k| = 3\text{m}^{-1}$.

Several features common to low frequency operation are illustrated in Fig. 3, where $\delta k = +3\text{m}^{-1}$. First, the profile modification due to the $k_2$ current is almost identical to the modification due to the $k_0$ current. This equality arises because these two currents have the same magnitude, and the field equations driven by the two transverse currents are virtually the same. Second, there is a sharp discontinuity at the beam edge, which reflects the beam surface charge and current given by Eq. 23 and 24. Of course, in the real world this discontinuity does not exist, and the discontinuity is instead manifested by a sharp field gradient. The gradients extend over the width of the beam undulation, and the total field change is approximately equal to the magnitude of the discontinuity. Third, the field profile due to $k_1$, the longitudinal space-charge wave current, is much larger than the field modifications due to the transverse currents. Since the space-charge wave is driven by terms proportional to $v_z$, the transverse modifications are driven by terms proportional to $v_w$, and since $v_w < v_z$, the space-charge wave will generally dominate the profile modification (at least at low frequencies).

However, since the gain $\delta k$ is proportional to $v_w$, the fraction of the mode profile modification due to the space-charge wave decreases as $\delta k \propto v_w$ is increased. Increasing the wiggler field while other parameters are held fixed also moves the FEL from the collective (Raman) regime into the Compton regime.

Figure 4 shows the profile for $\delta k = -3\mathrm{m}^{-1}$. The results are similar to the $\delta k = 3\mathrm{m}^{-1}$ case, except as expected, the profiles are inverted. For real values of $\delta k$, the profiles for each of the three wavenumbers $k_0$, $k_1$, and $k_2$ are either pure real or pure imaginary, but for imaginary values of $\delta k$ the profiles are complex as shown in Fig. 5. Here the major profile modification for the $k_0$ and $k_2$ terms is a phase shift across the waveguide. Even for imaginary values of $\delta k$, however, the mode profile modifications are still dominated by the space-charge wave fields.

The total time averaged electric field profiles are shown in Fig. 6 for $\delta k = 1\mathrm{m}^{-1}$ and $\delta k = i\mathrm{m}^{-1}$. The uppermost profiles are at $z = 0$cm, and each succeeding profile is spaced by $\Delta z = l_w/8 = 0.4125$cm. Large variations with $z$ are observed for $E_r$, but only small variaions in $E_\phi$ and $E_z$. For $\delta k = 1\mathrm{m}^{-1}$, at $z = l_w/4$ and at $z = 3l_w/4$ the space-charge wave component $k_1$ is asymmetric and dominates the mode profile, but at $z = 0$ and $z = l_w/2$ the space charge wave phase is orthogonal to the RF wave phase and its contribution is small and symmetric. The surface boundary discontinuity is strongest at $z = l/4$ and $z = 3l_w/4$ because here the contributions from the $k_0$ and $k_2$ currents add in phase. At $z = 0$ and at $z = l_w/2$, however, the contributions from these two currents are out of phase and the boundary discontinuity disappears. Similar behavior is observed for $\delta k = i\mathrm{m}^{-1}$.

## B. Field profile with multiple FEL modes

The initial conditions at the FEL interaction region entrance split the input power into several modes. In one dimensional theory, each mode has a wavenumber shift $\delta k_i$ which is a solution of the dispersion relation Eq. 29. The fraction of the input power in each of the three $\delta k_i$ modes is given[24] by the residues $\mathcal{R}_i$, where

$$\mathcal{R}_i = \mathrm{Res}\left[\frac{(\delta k - \Theta + \Theta_p)(\delta k - \Theta - \Theta_p)}{\delta k(\delta k - \Theta + \Theta_p)(\delta k - \Theta - \Theta_p) + Q}\right]_{\delta k = \delta k_i} \qquad (30)$$

The total electric field is then given by

$$E_{1d} = \sum_{i=1}^{3} \mathcal{R}_i e^{i(\omega t - (k_z + \delta k_i)z)}. \tag{31}$$

Note that the residues satisfy (and can alternately be found from) the three conditions

$$1 = \sum_{i=1}^{3} \mathcal{R}_i, \tag{32}$$

$$0 = \sum_{i=1}^{3} \mathcal{R}_i \delta k_i, \tag{33}$$

$$0 = \sum_{i=1}^{3} \mathcal{R}_i \delta k_i^2. \tag{34}$$

These equations express the requirement that the electric field at $z = 0$ sums to unity, and that the first and second derivative of the field at $z = 0$ is zero. (Alternately that the beam is initially unperturbed).

In the collective regime the one dimensional behavior is normally dominated by one or two of the FEL modes; in the strong pump regime all three modes can be important. Of course, if there is substantial net gain in the system, only the growing mode is important. Consequently, for high net gain, the three dimensional field will be dominated by only one mode, and the solution of the previous section can be used. However, we will show that in the low net gain case, for both the collective and strong pump regimes, the complete three dimensional field profile always depends on all three FEL modes.

The three dimensional field profile is found by adding together appropriate contributions from each FEL mode. Specifically, for a given set of FEL parameters, we first solve for the three distinct sets of $\delta k_i$ and $\mathcal{R}_i$. Next the field profiles for each of these individual $\delta k_i$ are determined. Finally, the three field patterns are superimposed, using the $\mathcal{R}_i$ as weights. Defining $\mathcal{U}(r, \phi)$ to be the unperturbed field profile, $\mathcal{P}_m(r, \phi, \delta k)$ to be the portion of the field profile modification at the position $(r, \phi)$, due to the wavenumber mode $m$, that results from a given value of $\delta k$, the field for a single FEL mode can be written as

$$\mathbf{E} = e^{i(\omega t - (k_z + \delta k)z)} \left[ \mathcal{U}(r, \phi) + \sum_{m=0}^{2} \mathcal{P}_m(r, \phi, \delta k) e^{-imk_w z} \right]. \tag{35}$$

Then the total field is found by summing over all the FEL modes:

$$\mathbf{E} = e^{i(\omega t - k_z z)} \left[ \mathcal{U}(r,\phi) \sum_{i=1}^{3} \mathcal{R}_i e^{-i\delta k_i z} + \sum_{i=1}^{3} \mathcal{R}_i e^{-i\delta k_i z} \sum_{m=0}^{2} \mathcal{P}_m(r,\phi,\delta k_i) e^{-imk_w z} \right]. \tag{36}$$

Since this sum involves nine different profiles, the behavior of the resulting solutions is quite complex.

Close examination of the single FEL mode solutions shows that the deviation from the unperturbed waveguide field depends almost linearly on $\delta k$. For the parameters of Figs. 3, and for $\delta k < 20\mathrm{m}^{-1}$, the non-linear component of the deviation is less than one percent of the total deviation. Thus we can assume that, to a good approximation,

$$\mathcal{P}_m(r,\phi,\delta k) = \delta k \tilde{\mathcal{P}}_m(r,\phi). \tag{37}$$

Using this substitution, the total field is

$$\mathbf{E} = e^{i(\omega t - k_z z)} \left[ \mathcal{U}(r,\phi) \sum_{i=1}^{3} \mathcal{R}_i e^{-i\delta k_i z} + \sum_{m=0}^{2} \tilde{\mathcal{P}}_m(r,\phi) e^{-imk_w z} \sum_{i=1}^{3} \mathcal{R}_i \delta k_i e^{-i\delta k_i z} \right] \tag{38}$$

or,

$$\begin{aligned} \mathbf{E} &= e^{i(\omega t - k_z z)} \left[ \sum_{i=1}^{3} \mathcal{R}_i e^{-i\delta k_i z} \right] \\ &\quad \times \left[ \mathcal{U}(r,\phi) + \frac{\sum_{m=0}^{2} \tilde{\mathcal{P}}_m(r,\phi) e^{-imk_w z} \sum_{i=1}^{3} \mathcal{R}_i \delta k_i e^{-i\delta k_i z}}{\sum_{i=1}^{3} \mathcal{R}_i e^{-i\delta k_i z}} \right]. \end{aligned} \tag{39}$$

Defining the composite $\delta k$ – scalar $\kappa$,

$$\kappa = \frac{\sum_{i=1}^{3} \mathcal{R}_i \delta k_i e^{-i\delta k_i z}}{\sum_{i=1}^{3} \mathcal{R}_i e^{-i\delta k_i z}}, \tag{40}$$

then

$$\mathbf{E} = e^{i(\omega t - k_z z)} \left[ \sum_{i=1}^{3} \mathcal{R}_i e^{-i\delta k_i z} \right] \left[ \mathcal{U}(r,\phi) + \kappa \sum_{m=0}^{2} \tilde{\mathcal{P}}_m(r,\phi) e^{-imk_w z} \right]. \tag{41}$$

Using the definition of $\tilde{\mathcal{P}}$ we can rewrite this as

$$\mathbf{E} = e^{i(\omega t - (k_z + \kappa) z)} \left[ e^{i\kappa z} \sum_{i=1}^{3} \mathcal{R}_i e^{-i\delta k_i z} \right] \left[ \mathcal{U}(r,\phi) + \sum_{m=0}^{2} \mathcal{P}_m(r,\phi,\kappa) e^{-imk_w z} \right]. \tag{42}$$

Except for the transversely independent factor $\left[e^{i\kappa z}\sum_{i=1}^{3}\mathcal{R}_i e^{-i\delta k_i z}\right]$, this expression is exactly equivalent to the field from a single value $\delta k = \kappa$. In other words, the complete mode profile, including the initial conditions and the three FEL modes, can be found by assuming that there is just one mode with the single composite $\delta k$ – scalar defined in Eq. 40.

The composite $\delta k$ – scalar can be alternately expressed as

$$\kappa = -i\frac{\partial}{\partial z}\ln\left(\sum_{i=1}^{3}\mathcal{R}_i e^{-i\delta k_i z}\right) = -i\frac{\partial}{\partial z}\ln\left(e^{-i(\omega t - k_z z)}\mathrm{E}_{1\mathrm{d}}\right). \qquad (43)$$

The composite $\delta k$ – scalar $\kappa$ has the intuitively plausible interpretation as the change with $z$ of the slowly varying amplitude of the 1-d solution. Alternately, using $\kappa$ to construct the mode profiles at some axial position $z$ is equivalent to using the following proceedure: First, determine the local electron beam density modulations in a region near $z$. Next, assume that the beam has an identical density modulation for all other values of $z$. Note that although this modulation is periodic, its amplitude can be growing or decaying if the local modulation on the original beam is growing or decaying. By construction, this modulation will produce an FEL wavenumber shift $\delta k$ exactly equal to the composite $\delta k$ – scalar $\kappa$. Finally find the mode profile at $z$ on the idealized beam. This calculated mode profile should be very close to the actual mode profile. Thus, using the composite $\delta k$ – scalar is equivalent to assuming that the local beam modulation persists in a region large enough that any transients in the profile associated with changes in $\kappa$ have died out. Formally,

$$1 \gg \frac{1}{\kappa k}\frac{\Delta\kappa}{\Delta z}. \qquad (44)$$

This relation is required by the eikonal approximation which underlies much FEL theory, and is usually satisfied.

For certain values of the detuning $\Theta$, one or two of the $\mathcal{R}_i$ may be close to zero. For example, for the experiments of Ref. 18, typical values of the roots and residues are 4.348, -3.821,-0.527 and 0.051, -0.085, 1.035 respectively. Since the last residue is at least twelve times greater than the first two residues, the one dimensional behavior is dominated by the last root, and the first two roots can be ignored without introducing any large errors. However, is not permissible to ignore these small roots in three dimensional

case. If we expand $\kappa$ in small $\delta k_i z$, we find

$$\kappa = \frac{\sum_i \mathcal{R}_i \delta k_i - i \sum_i \mathcal{R}_i \delta k_i^2 z - \sum_i \mathcal{R}_i \delta k_i^3 z^2 + \ldots}{\sum_i \mathcal{R}_i - i \sum_i \mathcal{R}_i \delta k_i z - \sum_i \mathcal{R}_i \delta k_i^2 z^2 + \ldots}. \tag{45}$$

Using the identities in Eqs. 32-34, this simplifies to

$$\kappa = -z^2 \sum_i \mathcal{R}_i \delta k_i^3. \tag{46}$$

Because roots with very little power (small $\mathcal{R}_i$), tend to have profiles very far from the unperturbed field profile (large $\delta k_i$), all the roots contribute approximately equally.

Equation 46 demonstrates that, as expected, the field profile modification at $z = 0$ is zero, and the profile modification grows parabolically with $z$. From Eq. 40, we see that when one of the roots corresponds to a growing mode, $\kappa$ quickly approaches the $\delta k$ of that mode. Unfortunately, no other general properties of $\kappa$ are evident. In Fig. 7 we plot $\kappa$ as a function of $z$ for several values of the detuning $\Theta$. The behavior of $\kappa$ is unpredictable; not only does $\kappa$ vary with $\Theta$, but even for fixed $\Theta$, $\kappa$ varies dramatically with $z$. However, as expected $\kappa$ approaches a constant when there is a growing mode (Fig 7c). For $\Theta = -\Theta_p$, destructive interference sharply reduces the output power at periodic values of $z$. At these points, the denominator of Eq. 40 approaches zero, producing a peak in $\kappa$ (Fig. 7a). Figure 8 shows $\kappa$ as a function of the detuning $\Theta$. Surveys of similar curves demonstrate that the only repeatable features are the peaks at the destructive detuning $\Theta$, and that $\kappa$ approaches $\delta k$ for growing mode. In Fig. 9, we plot the the total electric field at a fixed $z$ as a function of $\Theta$ at two transverse positions. Just as in the single mode case, the fields depend strongly on the phase of the wiggler at the measurement position. The two characteristic behaviors are fields slightly larger or smaller than the unperturbed field, or fields that lead or lag the unperturbed field.

Note that the residues $\mathcal{R}_i$ were found using one dimensional theory and will be slightly different when three dimensional effects are taken into account. The expansion Eq. 46 for $\kappa$ may then have a term linear in $z$, but the effect of this term can often be expected to be negligible.

## C. Nonlinear Interaction Field Profiles

The previous sections have assumed that the FEL was operating in the linear regime, but this assumption is not fundamental. Once the one dimensional nonlinear solution is determined by a numerical simulation, the alternate definition of the $\kappa$ given in Eq. 43 can be readily applied. In Fig. 10 we show the output power, phase and the real and imaginary parts of the composite $\delta k$ – scalar from a simulation of an FEL operating at 1.5mm wavelength with a 1.5kA, 2.13kV beam. The power grows exponentially, saturates at about 2.0 meters and undergoes synchrotron oscillations, and the FEL induced RF phase shift grows nearly linearly. The behavior of both the real and imaginary components of $\kappa$ is, however, rather complicated.

# IV. Scaling and self consistancy

In Fig. 11, we scan the beam radius at fixed gain, and plot the time averaged electric field. Since we hold the gain $\delta k$ constant, the beam must be more "active" per unit area for a small beam then for a large beam, and the deformations are indeed largest for the smallest beam. This effect can be understood somewhat more quantitatively by calculating an effective isotropic dielectric constant for the beam, as discussed in the introduction. Since this naive model predicts that the dielectric model is inversely proportional to the beam radius squared, the edge discontinuity should likewise be inversely proportional to the beam radius squared, in rough agreement with the curves of Fig. 11.

So far we have concentrated on frequencies that are not highly overmoded. In Fig. 12, we show the time averaged electric fields for frequencies up to 90GHz. The beam edge discontinuity remains roughly constant, reflecting the fact that the surface charge and current magnitudes are independent of the frequency, and the wiggling velocity, $v_w$, has been held fixed (Eq. 23). The transverse inhomogeneous fields are likewise independent of frequency. However, the space-charge wave magnitude is inversely proportional to frequency. Since the ratio of the beam radius to the waveguide radius remains fixed at 0.2, and since the radiation is constrained to be in a $TE_{11}$ like mode, the profile does not necessarily approach that of a standard, high frequency, optically guided mode.

Our model assumes that the wavenumber shift due to the FEL interaction $\delta k$ is known. The field profiles are then calculated from the resulting current profile. The model is not self-consistent since the transverse field profiles used in calculating $\delta k$ do not include the influence of the FEL interaction. An improved estimate of the FEL growth rate could be made by iterating the present scheme—using the new field profiles to obtain a new FEL growth rate.

## V. Conclusions

In this paper we study the waveguide analog of optical guiding in a free electron laser by finding the the fields produced by a bunched, undulating electron beam. The beam density modulation produces both radial and axial space-charge field components at the ponderomotive wavenumber $k_z + k_w + \delta k$, and the coupling of the modulation and the beam undulation yields field components at wavenumbers $k_z + \delta k$ and $k_z + 2k_w + \delta k$. The complete transverse electric field is determined by the superposition of these field components. We show, for the parameters of a microwave FEL, that the mode profiles have a rich transverse structure. The analysis yields profiles which are strongly influenced by both the radial component of the space charge field at wavenumber $k_z + k_w + \delta k$, and by discontinuities at the beam boundary which arise from the surface charge and surface current terms at $k_z + \delta k$ and $k_z + 2k_w + \delta k$. (In a realistic beam with a smooth edge density profile, these discontinuities would be spread out over the beam boundary region). The fields generally have profiles that, depending on the axial position relative to the phase of the wiggler, transform through eight distinct shapes. The analysis is dependent on the FEL induced wavenumber shift $\delta k$, which is found by solving the standard FEL cubic equation.[24] When the gain is high, only one root of this equation is needed; however, at low gain, all three FEL modes need to be included, and an expression for a composite $\delta k$ – scalar is employed to find the three dimensional fields. The expression for the composite $\delta k$ – scalar is equivalent to the logarithmic derivative of the complex eikonal electromagnetic field. This alternate definition of $\delta k$ is employed to extend the analysis to the nonlinear regime.

We find, consistent with the simple "epsilon" fiber model discussed in the introduction, that the profile modifications at low frequencies are large. As

expected, the size of the modifications decreases with the beam radius (at fixed gain). This results in a larger perturbation of the mode near the electron beam. The space charge wave components decrease at high frequencies, but the beam edge discontinuity does not.

Experiments have measured[14] the transverse field structure inside an FEL. Direct comparisons of these measurements with our theory are not possible because the experiments use a rectangular waveguide, and because the probes used in the experiments are not entirely unidirectional. Nonetheless, we find some qualitative agreement between theory and the experiment. For example, the space charge fields dominate the transverse profile m i-ifications. The profile modifications exhibit inversion symmetry when the measurement position is shifted by half the wiggler period. Leads and lags between field amplitudes measured at different transverse positions are both predicted and observed.

## VI. Acknowledgements

We acknowledge useful discussions with G. Bekefi, A. Fruchtman, F. Hartemann, E. Jerby, N. Kroll, B. Thompson and K. Xu. This work has been supported by the National Science Foundation, the Office of Naval Research, and the Department of Energy, Office of High Energy Physics.

## References


[1]H. Motz, J. Appl. Phys.**22**, 527 (1951).

[2]R. M. Phillips, *IRE Trans. Electron Devices* **ED-7**, 231 (1960).

[3]C. W. Roberson and P. Sprangle, to be published in *Phys. Fluids* **B1** 1 (1989).

[4]T.J. Orzechowski, E. T. Scharlemann, B. Anderson, V. K. Neil, W. M. Fawley, D. Prosnitz, S. Yarema, D. B. Hopkins, A. C. Paul, A. M. Sessler, and J. S. Wurtele, *IEEE Jour. Quan. Electron.* **QE-21**, 831 (1985).

[5]J. Fajans, J. S. Wurtele, G. Bekefi, D. S. Knowles, and K. Xu, Phys. Rev. Lett.**57**, 579 (1986).

[6]H. Haus, Electrodynamics Memo 101, Research Laboratory of Electronics, Massachusetts Institute of Technology, Cambridge, 1980.

[7]N. M. Kroll, P. L. Morton, and M. R. Rosenbluth, *IEEE J. Quantum Electron.* **QE-17**, 1436 (1981).

[8]D. Prosnitz, A. Szoke, and V. K. Neil, *Phys. Rev. A* **24**, 1436 (1981).

[9]P. Sprangle and C. M. Tang, *Appl. Phys. Lett.* **39**, 677 (1981).

[10]G. T. Moore, Opt. Commun.**52**, 46 (1984).

[11]E. T. Scharlemann, A. M. Sessler, and J. S. Wurtele, Phys. Rev. Lett.**54**, 1925 (1985).

[12]T. J. Orzechowski, E. T. Scharlemann, and B. D. Hopkins, Phys. Rev. A**35**, 2184 (1987).

[13]A. Battacharjee, S. Y. Cai, S. P. Chan, J. W. Dodd, and T. C. Marshall, Phys. Rev. Lett.**60**, 1254 (1988).

[14]F. Hartemann, K. Xu, G. Bekefi, J. S. Wurtele, and J. Fajans, Phys. Rev. Lett.**59**, 1177 (1987).

[15]J. E. Lasala, D. A. G. Deacon, and J. M. J. Madey, Phys. Rev. Lett.**59**, 2047 (1987).

[16]B. E. Newnam, R. W. Warren, R. L. Sheffield, J. G. Goldstein, and C. A. Brau, *Nucl. Inst. and Meth. in Phys. Rev. A* **237**, 187 (1985).

[17]R. A. Waldron, **The Theory of Cavity Waveguides**, (Mackaren and Sons, London, 1967), p. 88.

[18]J. Fajans and G. Bekefi, *Phys. Fluids* **29** 3461 (1986).

[19]J. Masud, T. C. Marshall, S. P. Schlesinger, and F. G. Yee, Phys. Rev. Lett., **56**, 1567 (1986).

[20]J. Mather and J. A. Pasour,Phys. Rev. Lett.**56**, 1805 (1986).

[21]E. Jerby and A. Gover, *Nucl. Instr. and Methods in Phys. Res.* **A272**, 380 (1988).

[22]H. Freund and A Ganguly, *Phys Rev. A* **28**, 3438 (1983).

[23]G. M. Branch and T. G. Mihran, *IRE Trans. Elec. Dev.* **ED-2**, 3 (1955).

[24]E. Jerby and A. Gover, *IEEE J. Quant. Electron.* **QE-19**, 1041 (1985).

[25]H. Uhm and R. C. Davidson, *Phys. Fluids* **24**, 1541 and 2348 (1981).

[26]E. T. Scharlemann, W. M. Fawley, B. R. Anderson, and and T. J. Orzerchowski, *Nucl. Instr. and Methods in Phys. Res.* **A250**, 150 (1985).

[27]J. S. Wurtele, E. T. Scharlemann, and A. M. Sessler, *Nucl. Instr. and Methods in Phys. Res.* **A250**, 176 (1985).

[28]A. K. Ganguly, and H. P. Freund, *Phys. Fluids* **31**, 387 (1988).

[29]J. Byers and R. Cohen, *Nucl. Instr. and Methods in Phys. Res.* **A272**, 595 (1988).

[30]S. Y. Cai, A. Battacharjee, and T. C. Marshall, *IEEE J. Quantum Electron.* **QE-23**, 1651 (1987).

[31]A. Fruchtman, *Phys. Rev. A*, **37**, 2989 (1988).

## Figures

Fig. 1 Beam and waveguide geometry.

Fig. 2 Decomposition of the true beam into a nonwiggling component and an edge component. For simplicity, the beam is undulated by a linear wiggler, and is assumed to be charge neutral.

Fig. 3 The field profiles (arbitrary units) vs. $x$ for $\delta k = +3\mathrm{m}^{-1}$. The dotted line is the unperturbed mode profile, and the solid, dot-dashed, and dashed lines are the profiles generated by the $k_0$, $k_1$, and $k_2$ currents respectively. The **R** and **I** respectively denote pure real and pure imaginary curves. Curves are not shown if they are everywhere equal to zero. (For example, the imaginary $k_0$, $\mathbf{E}_x$ field, or the $k_1$, $\mathbf{E}_y$ field.) The horizontal tick marks indicate the position of the beam.

Fig. 4 The $\mathbf{E}_x$ field profile vs. $x$ for $\delta k = -3\mathrm{m}^{-1}$. The remaining field components are similarly inverted with respect to the profiles of Fig. 3. The curves are identified as in Fig. 3.

Fig. 5 The real part (a) and the imaginary part (b) of the $\mathbf{E}_x$ field profile vs. $x$ for $\delta k = 3i\mathrm{m}^{-1}$. The curves are identified as in Fig. 3.

Fig. 6 The total electric field profiles vs. $x$ with $\delta k = 1\mathrm{m}^{-1}$ (a, b, c, d) and $\delta k = i\mathrm{m}^{-1}$ (a$\prime$, b$\prime$, c$\prime$, d$\prime$). Graphs are equally spaced in $z$ such that (a, a$\prime$) is at $z = 0$, (b, b$\prime$) is at $z = l_w/8$, (c, c$\prime$) is at $z = l_w/4$, and (d, d$\prime$) is at $z = 3l_w/8$. The solid curve is the $E_x$ field, the dashed curve is the $E_y$ field, and the dotted curve is the $E_z$ field. Graphs for $z = l_w/2$, $z = 5l_w/8$, $z = 3l_w/4$, and $z = 7l_w/8$, are identical to the curves shown except for a horizontal reflection through the center of the graphs. Other parameters are as in Fig. 3.

Fig. 7 The composite $\delta k$ – scalar $\kappa$ as a function of $z$ for $\Theta = -4.11\mathrm{m}^{-1}$ (a), $\Theta = 0\mathrm{m}^{-1}$ (b), and $\Theta = 4.11\mathrm{m}^{-1}$ (c). The real part of $\kappa$ is given by the solid line, and the imaginary part is given by the dashed line. The coupling constant $Q = 3.56\mathrm{m}^{-3}$ is adjusted to give a gain of 1.5 at $z = 1.0\mathrm{m}$, and the normalized plasma frequency is $\Theta_p = 4.11\mathrm{m}^{-1}$.

Fig. 8 The composite $\delta k$ – scalar $\kappa$ vs. the detuning $\Theta$. The real part of $\kappa$ is given by the solid line, and the imaginary part is given by the dashed line. For reference, the gain is given by the dotted line. The coupling constant is $Q = 3.56\mathrm{m}^{-3}$, the normalized plasma frequency is $\Theta = 4.11\mathrm{m}^{-1}$, and

$z = 1.7$m.

Fig. 9 Total electric field vs. the detuning $\Theta$. The field is plotted at $z = 0.99$m (a), $z = 0.99 + l_w/4$ (b),$z = 0.99 + l_w/2$ (c), $z = 0.99 + 3l_w/4$ (d). The solid line is the electric field at $x = 0.26$cm, just outside the beam, and the dashed line is the field at the wall. To the width of the lines, the field at the waveguide wall is identical to the field in the center. The coupling constant $Q = 6.39\text{m}^{-3}$ is adjusted to give a gain of 2 at $z = 1$m. Other parameters are as in Fig. 3.

Fig. 10 Output power (a), phase (b), and the real(c) and imaginary (d) parts of the composite $\delta k -$scalar vs.$z$ from a nonlinear simulation of an FEL operating at 1.5mm wavelength with a 1.5kA, 2.13kV beam. The power (a), and phase (b) behave smoothly compared with the Re$\kappa$ (c) and Im$\kappa$ (d).

Fig. 11 Electric field vs. $x$ for various beam radii $b = 0.1, 0.2, 0.5, 1.0$ cm. The discontinuities are at the beam edge, and identify the radius associated with each curve. The field is plotted at $z = l_w/8$, with a $\delta k = 0.75$. Other parameters are as in Fig. 3.

Fig. 12 Electric field vs. $x$ for the frequencies $f = 10, 50, 90$ GHz (solid, dashed dotted, respectively). The field is plotted at $z = l_w/8$, with a $\delta k = 0.75$. Other parameters are as in Fig. 3.

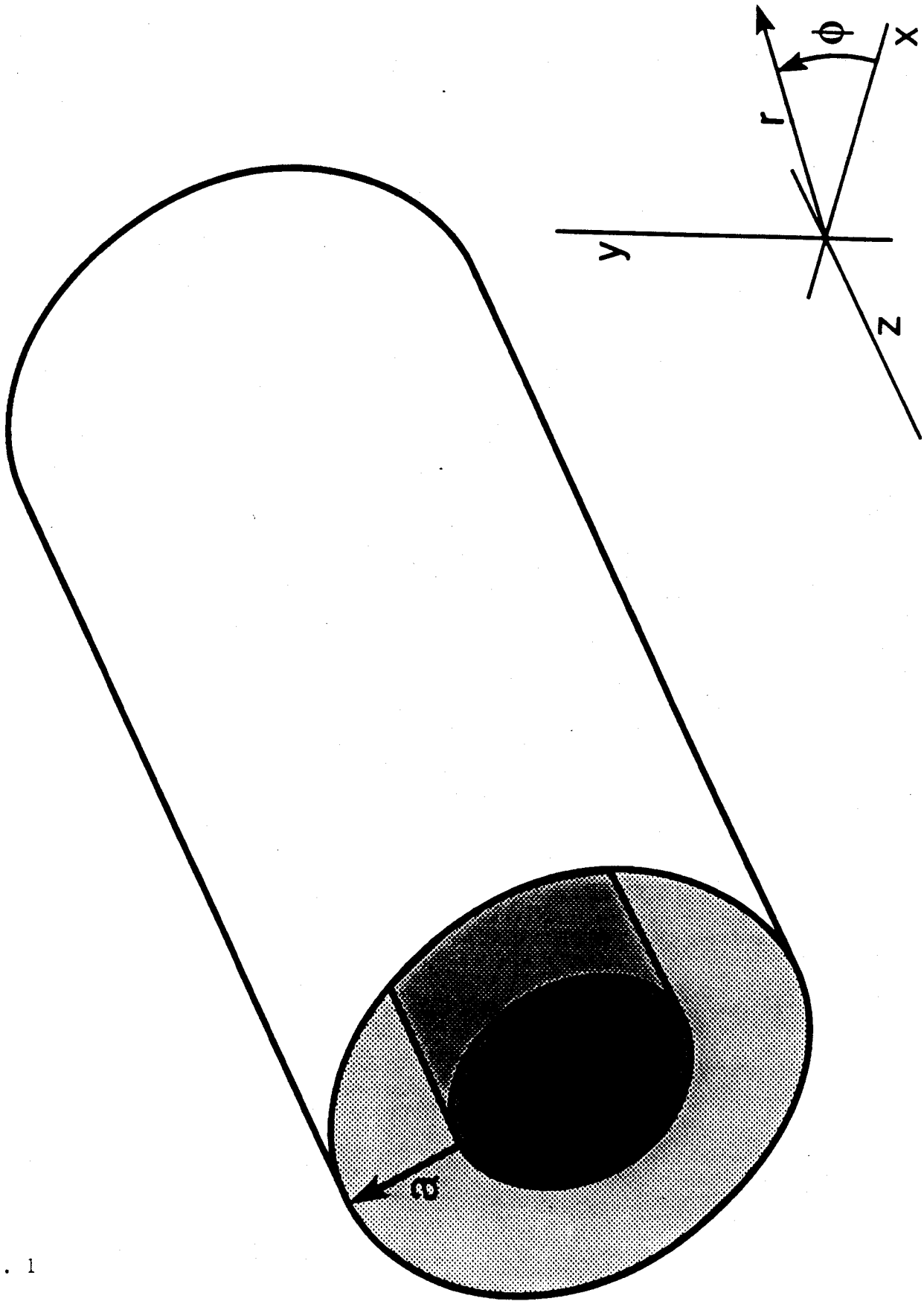


Fig. 1

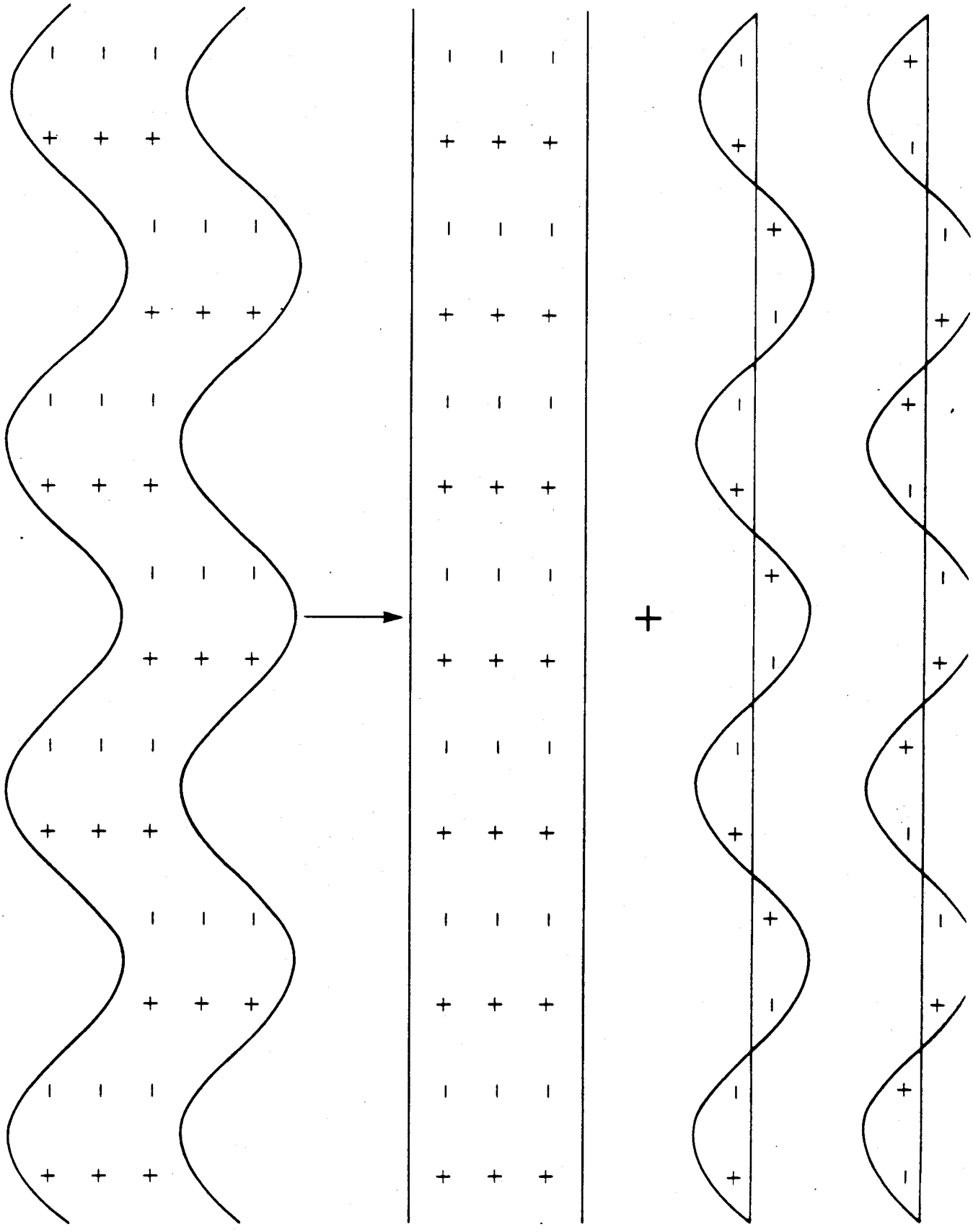

Fig. 2

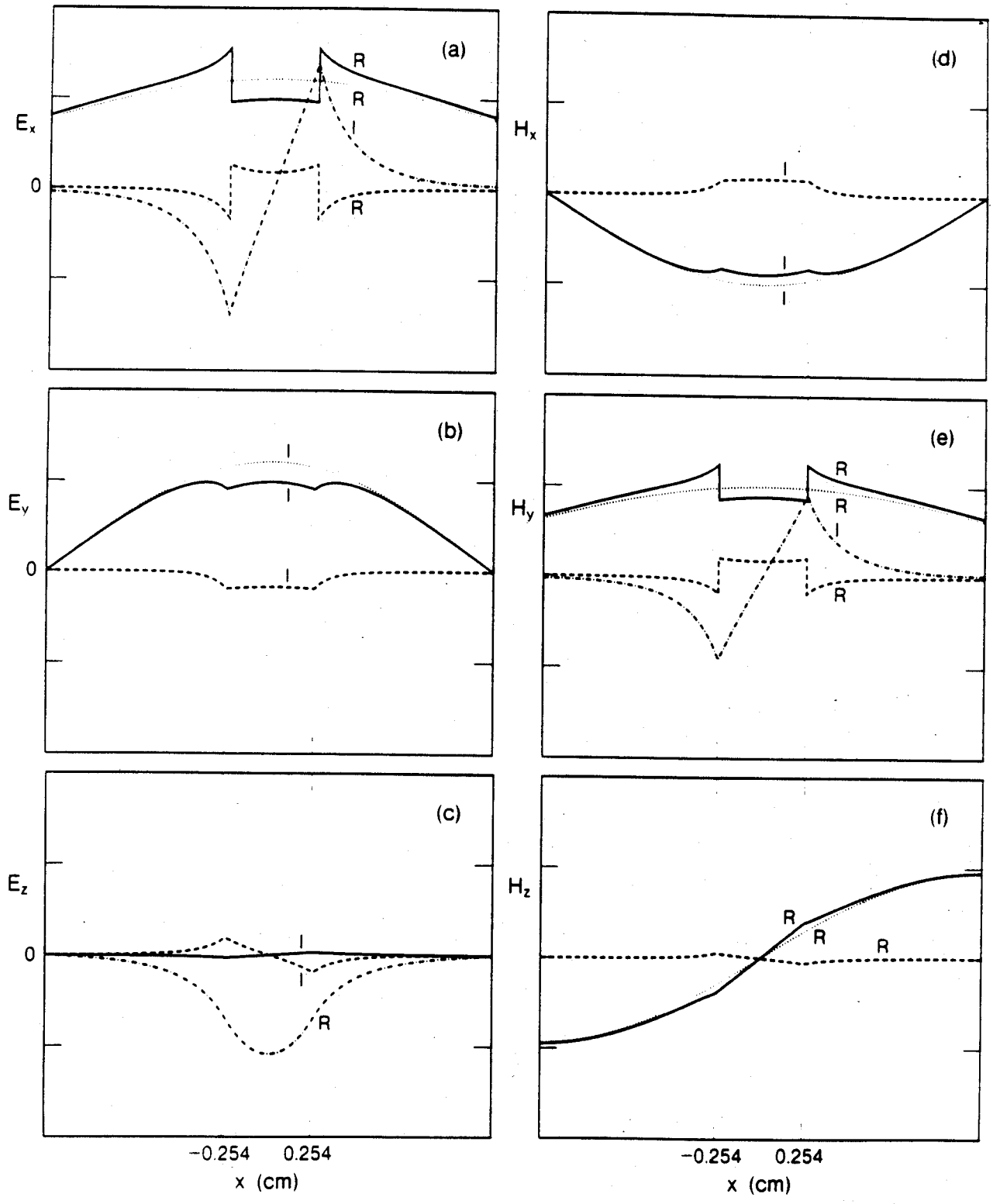


Fig. 3

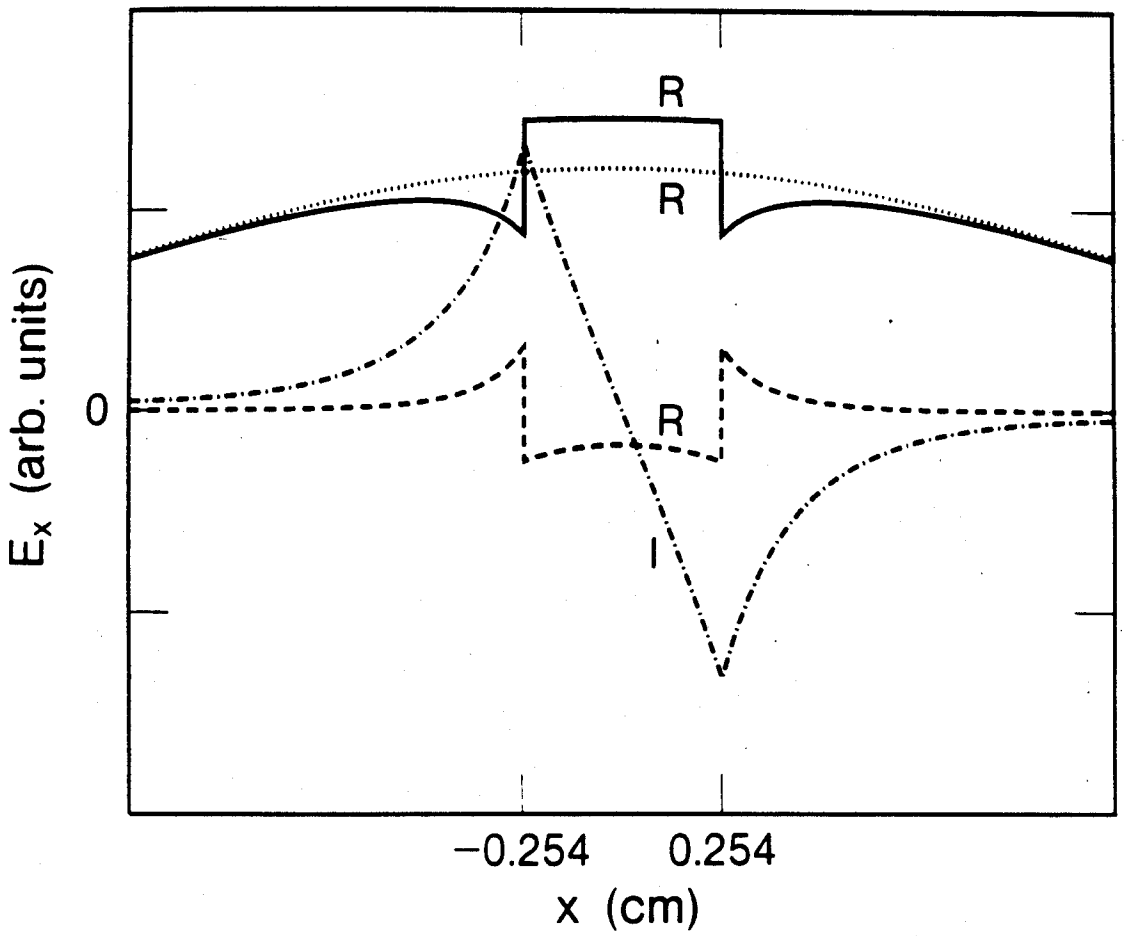


Fig. 4

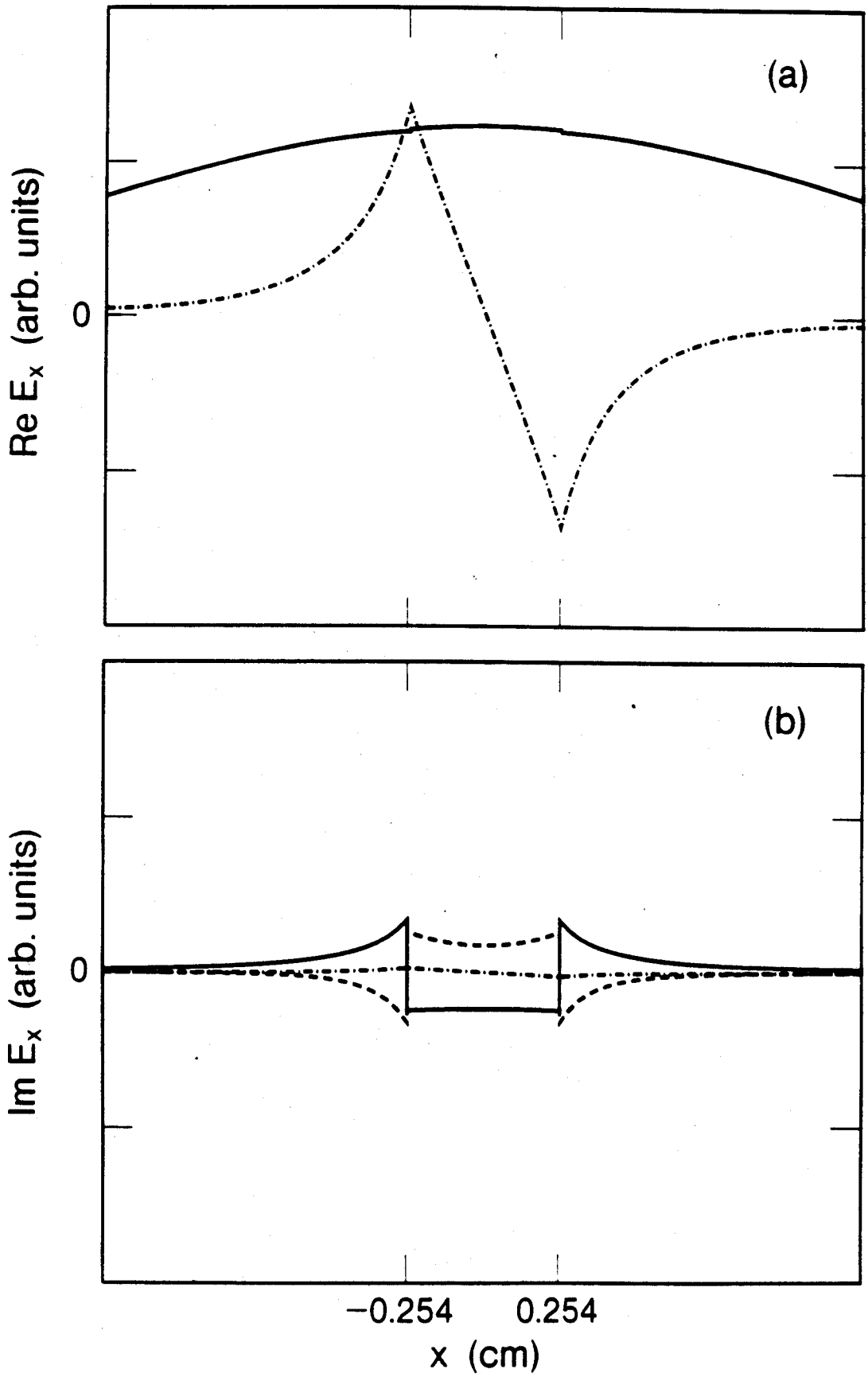


Fig. 5

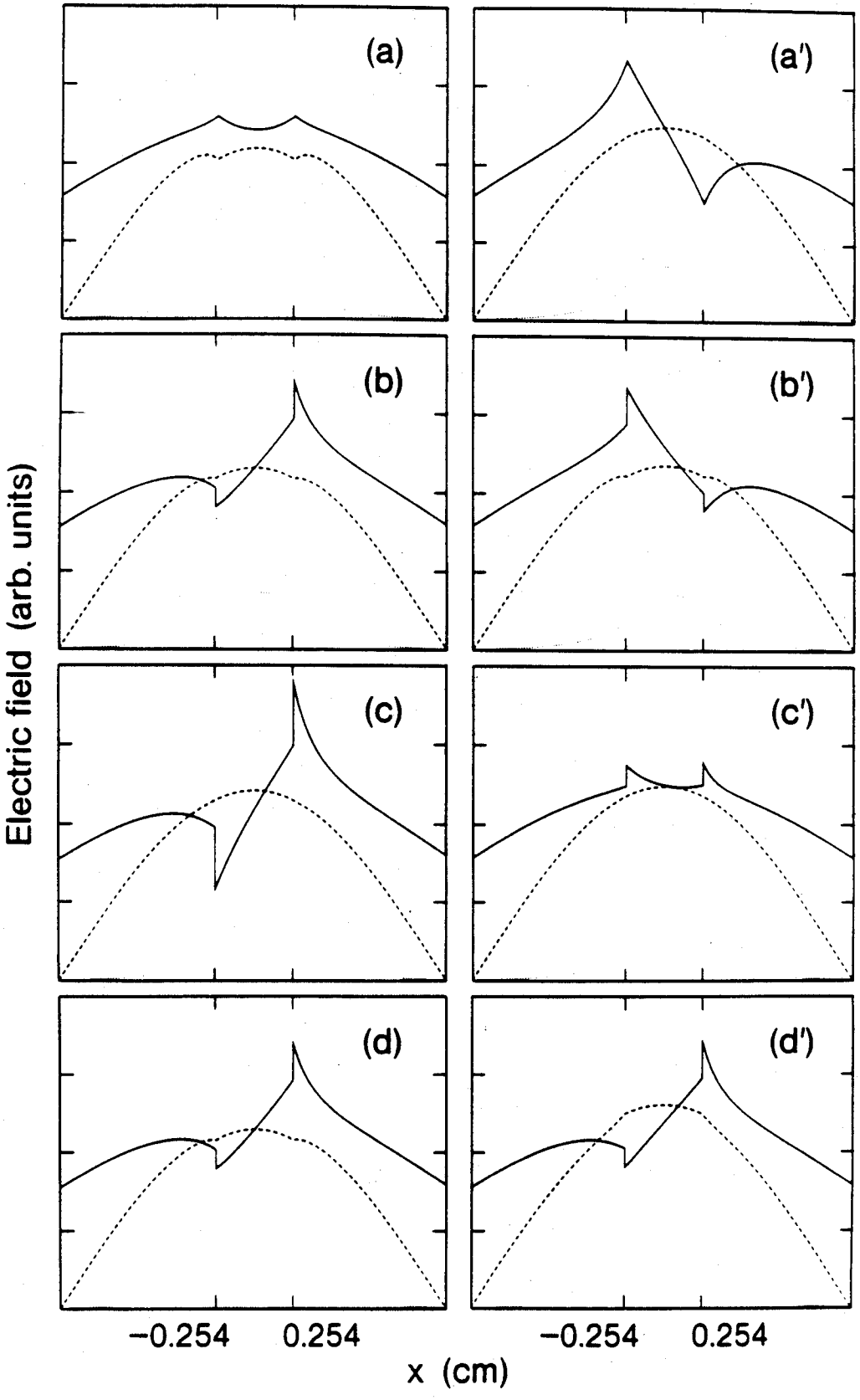


Fig. 6

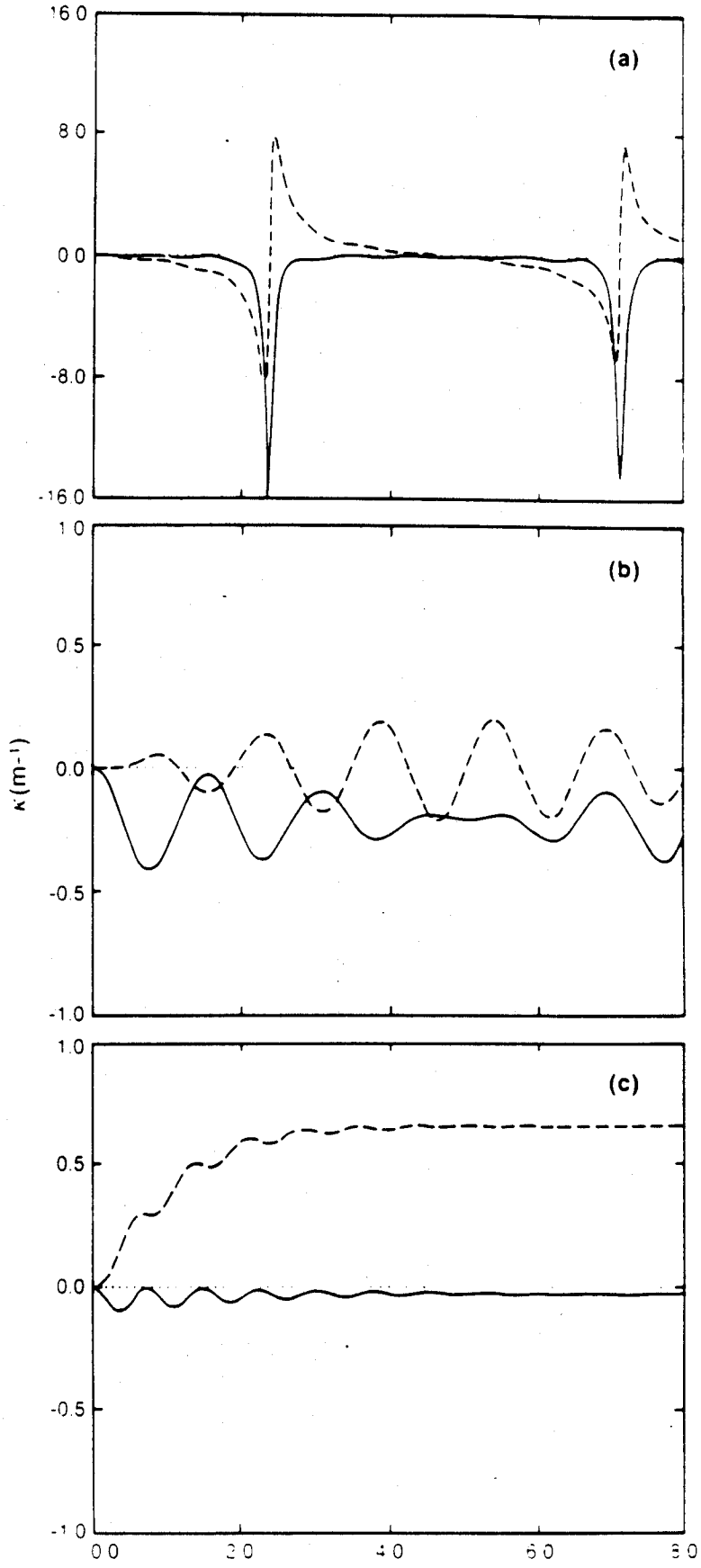
16.0
8.0
0.0
-8.0
-16.0
(a)
1.0
0.5
0.0
-0.5
-1.0
(b)
κ(m⁻¹)
1.0
0.5
0.0
-0.5
-1.0
(c)
0.0
2.0
4.0
6.0
8.0
Z(m)

Fig. 7

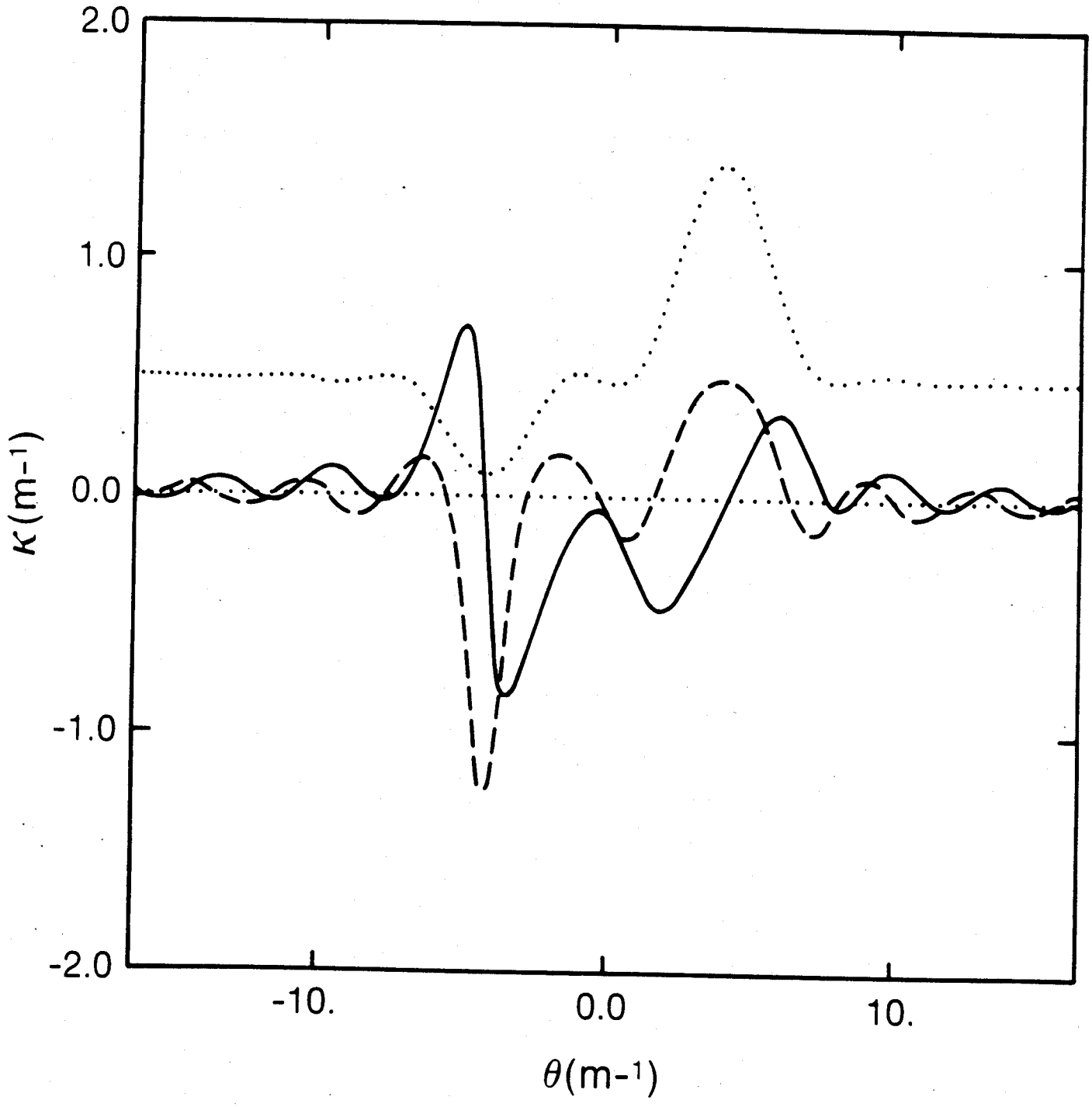


Fig. 8

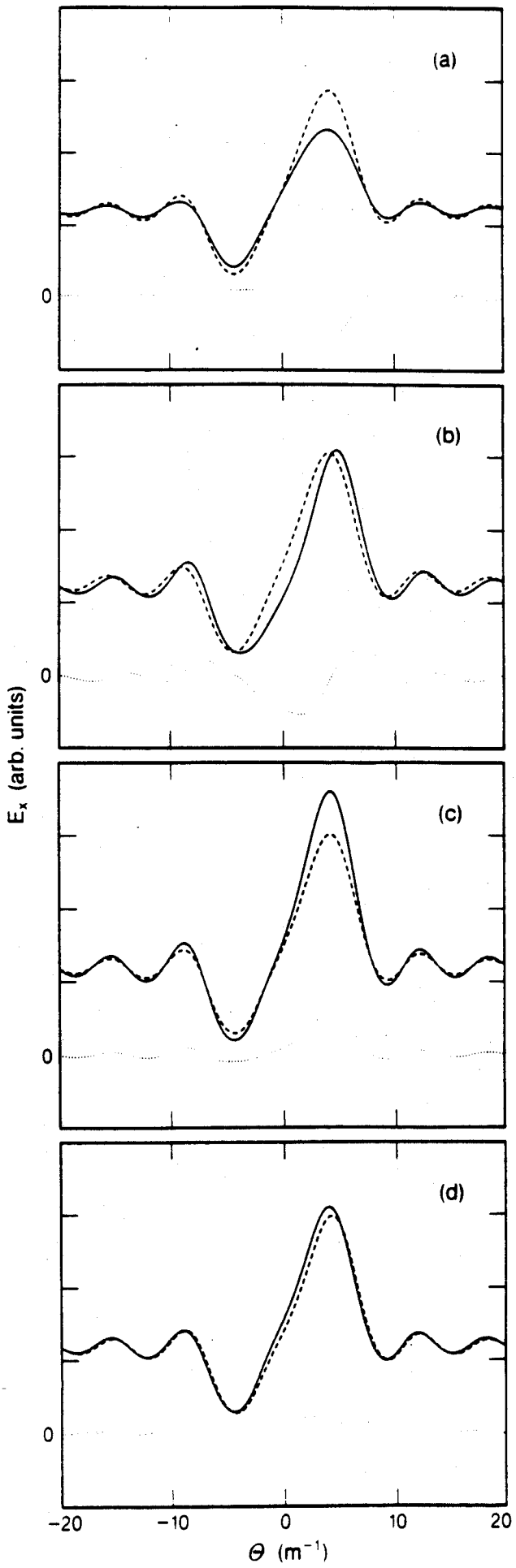


Fig. 9

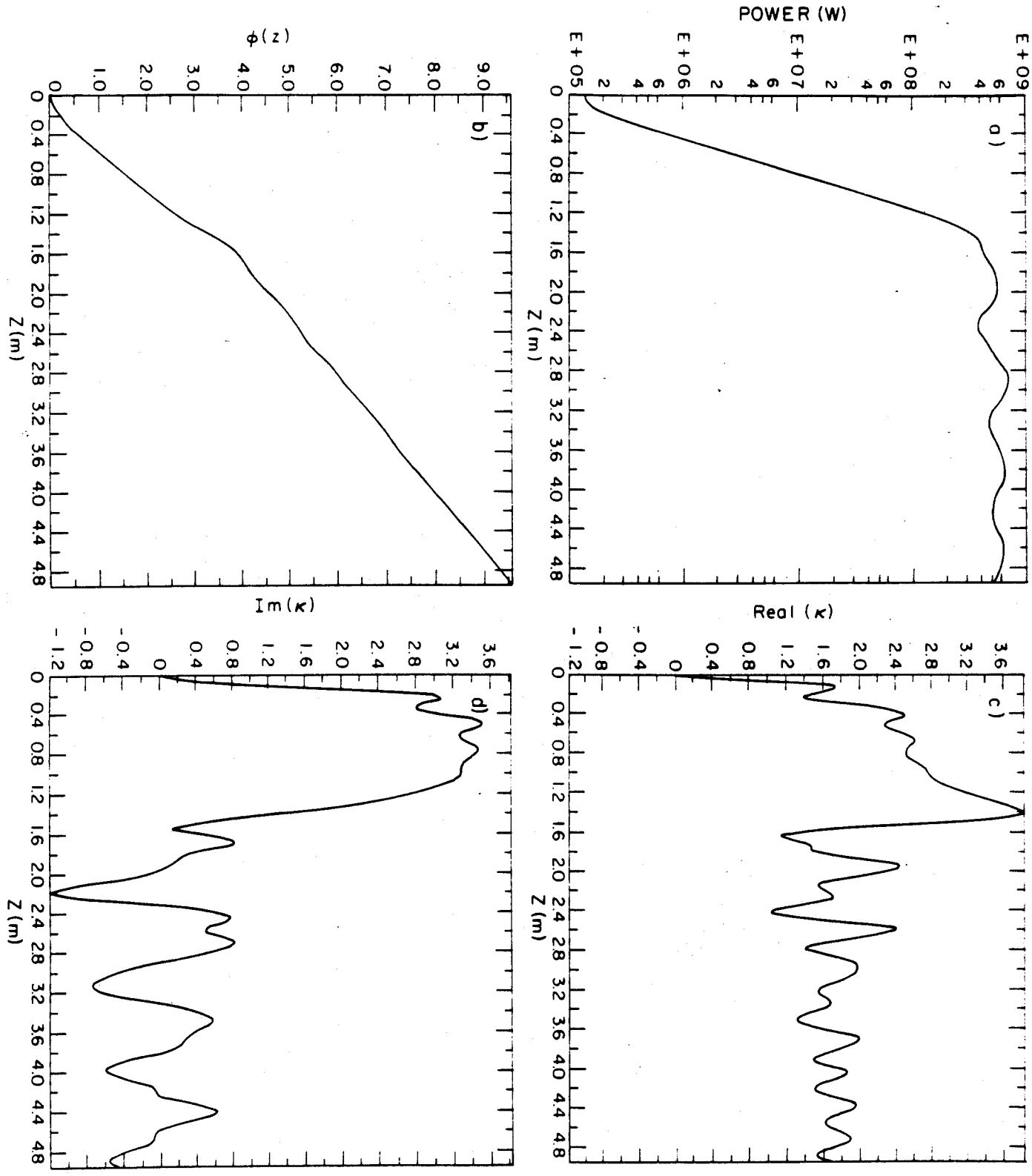


Fig. 10

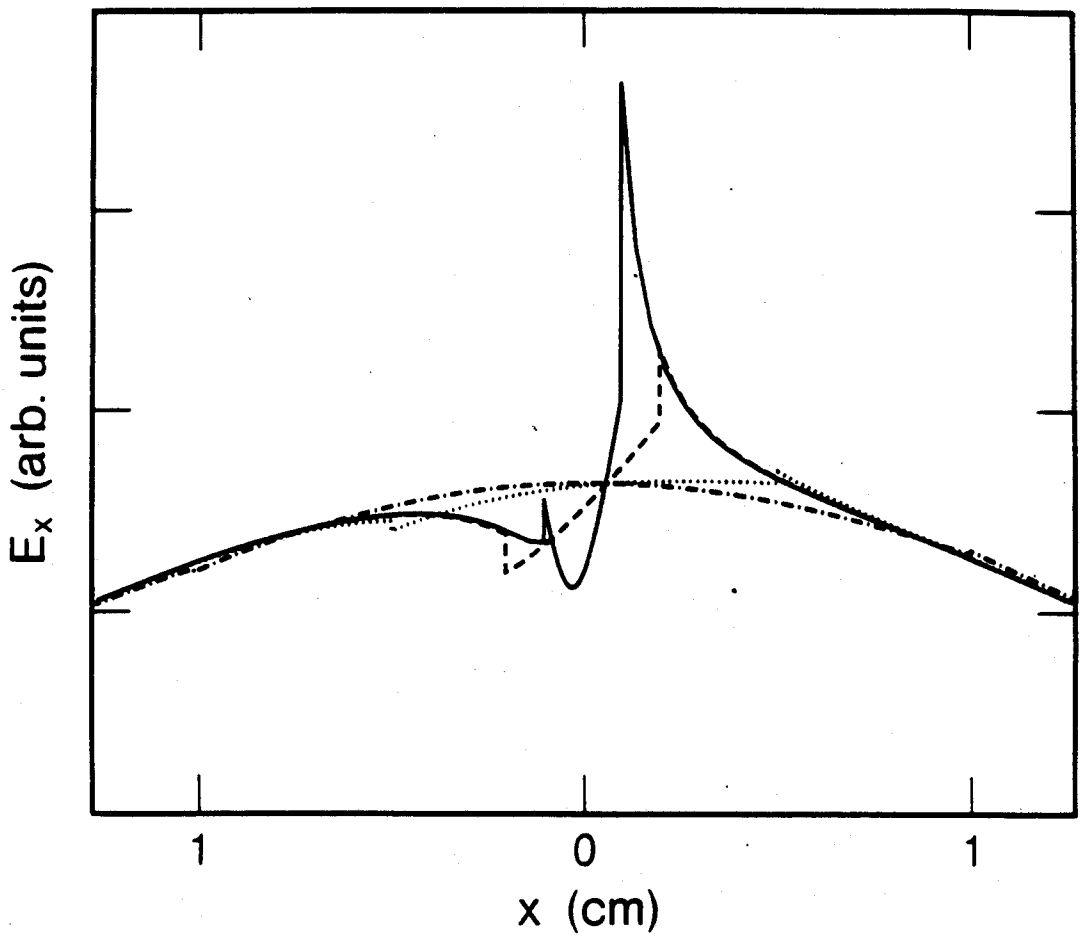


Fig. 11

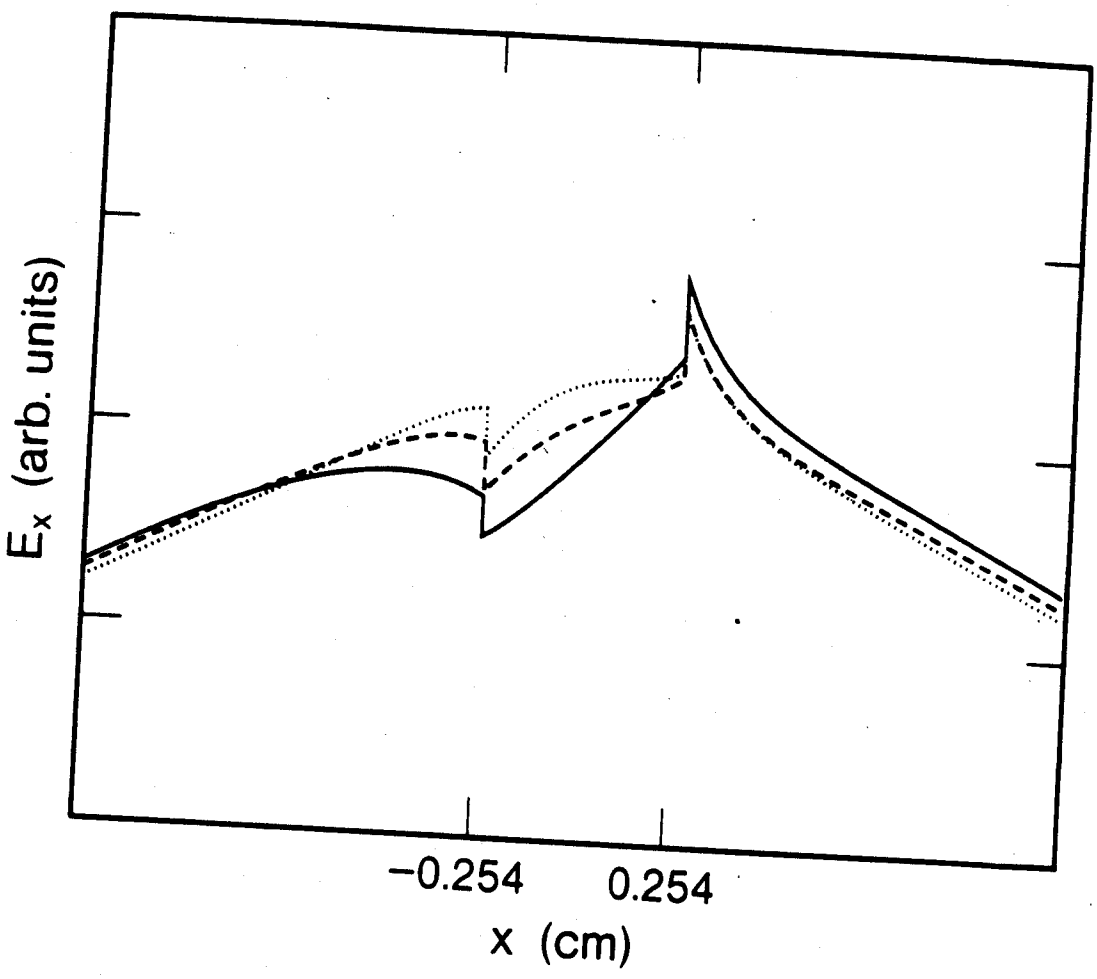


Fig. 12